Reaching the Yield Point of a Glass During X-Ray Irradiation

Alessandro Martinelli,[1,*] Federico Caporaletti,[2] Francesco Dallari,[1] Michael Sprung,[3] Fabian Westermeier,[3] Giacomo Baldi,[4] and Giulio Monaco[1,†]

[1]University of Padova, Department of Physics and Astronomy "Galileo Galilei," Via F. Marzolo, 8-35131 Padova, Italy
[2]Laboratory of Polymer and Soft Matter Dynamics, Experimental Soft Matter and Thermal Physics (EST), Université libre de Bruxelles (ULB), Brussels, 1050, Belgium
[3]Deutsches Elektronen-Synchrotron DESY, Notkestrasse 85, 22607 Hamburg, Germany
[4]University of Trento, Department of Physics, I-38123, Trento, Italy

(Received 26 January 2023; revised 7 August 2023; accepted 18 September 2023; published 15 November 2023)

A solid loaded beyond the yield stress loses its elastic properties and becomes plastic. From a microscopic point of view, this limit corresponds to the condition where plastic regions become so densely packed that they give rise to system-spanning structures. This limit for glasses is abrupt, which makes experimental investigations challenging. Here, the yield point is reached by the alternative approach of increasing the density of plastic regions by generation of point defects during x-ray irradiation. For the case of a $LiBO_2$ glass, we show that at low doses, i.e., for a low density of defects, the defects behave as isolated stress sources that induce atomic displacements typical of an elastic solid. As the density of defects increases, the mechanical response of the glass at the local scale changes from elastic to more and more plastic, until reaching the limit where it becomes characteristic of a flowing system, which signals that the yield point is reached.

DOI: 10.1103/PhysRevX.13.041031

Subject Areas: Condensed Matter Physics, Materials Science, Soft Matter

I. INTRODUCTION

A textbook approach to studying mechanical properties of a material is via the stress-strain curve, e.g., the strain response following an imposed stress. While this curve can be complex and material dependent, two regimes are well known. The first appears at low stress, where strain is proportional to stress: Here, the material undergoes an overall elastic deformation. The other regime appears further up along the curve and corresponds to the initiation point of plastic deformation. The stress component at this point is the yield stress. Understanding the mechanisms at play at yield is of utmost importance in materials science [1], with particular reference to the quest to develop prediction capabilities of material failure. Yielding also represents a central problem in statistical physics [2], focusing on the nature of this transition between an elastic solid and a flowing system [3–5].

In glasses, the situation is particularly challenging. First, some level of plastic response appears instantaneously for any amount of strain, even in the linear stress-strain region [6]. Moreover, following the increase in plastic activity towards the yielding transition is complicated by the fact that even the mere definition of a plastic region—which in crystalline materials is associated to a dislocation—is not trivial: In glasses, it is rather related to local, sliplike rearrangements of a few atoms known as shear transformation zones [7]. Thus, the identification of plastic rearrangements is very challenging both in experiments and simulations since they appear at a very small scale and the internal structure is statistically unchanged before and after the transformation [8].

Numerical simulation studies have associated shear transformation zones to regions where atomic motions are strongly nonaffine, i.e., with additional displacements on top of those dictated by the macroscopic strain [9]. Shear transformation zones are often modeled as inclusions in an elastic continuum using the famous analytic solution of Eshelby [10]. The macroscopic behavior of an amorphous system is then described in terms of an ensemble of Eshelby inclusions. The Eshelby displacement field is peculiar in its form: It decays as an elastic dipole and is highly anisotropic. This anisotropy leads to a preferential localization of the plastic activity along certain directions and plays a major role. For instance, as shear transformations build up, they tend to form shear bands [11], the main mechanism for mechanical failure in metallic glasses.

*alessandro.martinelli@unipd.it
†giulio.monaco@unipd.it

Published by the American Physical Society under the terms of the Creative Commons Attribution 4.0 International license. Further distribution of this work must maintain attribution to the author(s) and the published article's title, journal citation, and DOI.

From an experimental point of view, exploring, at the microscopic scale, the mechanical properties of glasses at yield is complicated by the difficulty of using imaging techniques with the required atomic resolution. Most of the available data refer, in fact, to soft matter where such limitations are relieved [12–14]. Moreover, glasses are brittle, the mechanical failure at yield is abrupt, and the characteristics of the yield transition depend significantly on the protocol used to prepare the material [5]. Thus, it is difficult to design schemes to test the theories that are currently being developed [15,16].

Here, we aim at looking at the evolution of plasticity in glasses using a different approach: We study the density fluctuations induced in a glass by defect generation during x-ray irradiation. We show here that the defects generated in the glass behave as dipolar sources of stress, thus playing the role of the plastic regions that develop in a glass under load. The x-ray dose allows us to control the density of defects in the glass. For a small density of defects, the atomic displacement field indicates that the defects are isolated and generate an elastic response of the surrounding medium. On increasing the density of defects, the response of the medium becomes more and more plastic, up to the point that it becomes, at the interatomic scale, that of a flowing glass at the yield point.

While the phenomenology under study here can be reported within the realm of material damage effects due to ionizing radiation, it is worth underlining some of its peculiar characteristics. In fact, classical beam damage usually refers to soft and biological matter, where the absorption of x rays triggers, in particular, the generation of free radicals, which in turn affect both the structural and dynamical properties of the system [17,18]. In that case, the damage typically increases continuously with the dose, and the main point of interest is to devise strategies to limit, if not avoid, the effects of beam damage in order to get access to the structural and dynamical properties of the system under investigation. The effect of interest here is peculiar for at least two reasons. (i) It leads to a dynamical response in a system (here, a $LiBO_2$ glass) that has no (slow) dynamics otherwise. In other terms, the measured dynamics is fully induced by the defects generated by the x-ray beam and can then be considered a perfect playground to study the effect of the generation of defects in the glass matrix. (ii) It is an effect that shows saturation to a stationary state. In fact, for a density of defects sufficiently high, a stationary state is reached where the generation of a new defect is accompanied by the healing of an existing one. This is the fully irradiated glass, which will be discussed in some detail in what follows.

The significance of the results reported here is then twofold. (i) Upon irradiation, glasses follow the entire transformation pathway, similarly to what happens in stress-strain experiments, from the elastic limit to the yield point. The generation of defects via x-ray irradiation can then be related to the mechanical generation of defects in more traditional stress-strain experiments. This offers an alternative tool to study the elasto-plastic response of glasses. Clearly, the glass at yield reached via irradiation is not the same glass reached at the yield point in stress-strain experiments: Our irradiated glass, for instance, does not show macroscopic flow. Still, its dynamical response at the interatomic scale is fully plastic. (ii) Coupling irradiation to the synchrotron-based technique of x-ray photon correlation spectroscopy, we obtain microscopic information on the mechanical response of glasses at the interatomic length scale relevant for the shear transformation zones mentioned previously. In particular, we can extract the distribution function of the atomic displacements induced by the generation of defects at different stages of irradiation, which correspond to different densities of defects. This information sheds new light on the evolution of the mechanical properties of glasses in the elasto-plastic regime. These results can therefore be of interest for theories and models, several of which are currently under development, attempting a full description of elasto-plasticity in amorphous materials [2].

II. RESULTS AND DISCUSSION

Our results are based on an x-ray photon correlation spectroscopy (XPCS) study of a $LiBO_2$ glass. XPCS probes the density correlation function, $F(q,t) = \langle \rho_q^*(0)\rho_q(t)\rangle$, where $\rho_q(t)$ is the Fourier q component of the microscopic density and q is the exchanged momentum [19]. In more detail, the scattered intensity is collected for a sequence of times by a pixelated 2D detector at a scattering angle θ, which defines the exchanged momentum via $q = (4\pi/\lambda)\sin(\theta/2)$, where λ is the wavelength of the incident x-ray beam. For each investigated θ, the angular resolution is chosen by dividing the detector image in regions of interest (ROI). The scattered intensity at a given time and for a pixel (p) belonging to a given ROI, $I_p(t)$, is then utilized to calculate the two-time correlation matrix:

$$C_q(t_1,t_2) = \frac{\langle I_p(t_1) I_p(t_2)\rangle}{\langle I_p(t_1)\rangle\langle I_p(t_2)\rangle}, \tag{1}$$

where $\langle\ldots\rangle$ is an average over the selected pixels. Equation (1) can alternatively be written in terms of the waiting time $t_w = t_1$ and lag time $t = t_2 - t_1$. Averaging $C_q(t_w, t_w + t)$ over t_w, we gain access to the function $g_2(q,t) = 1 + A|F(q,t)|^2$, where A is an instrumental constant known as the contrast [19,20]. Phenomenologically, $|F(q,t)|^2$ can be described by the so-called Kohlrausch-Williams-Watts (KWW) function [21]:

$$|F(q,t)|^2 = f_q^2 \exp[-2(t/\tau(q))^{\beta(q)}], \tag{2}$$

where $\tau(q)$ is the relaxation time, $\beta(q)$ the shape parameter, and f_q the strength of the relaxation process. In the following,

we will not evaluate A and f_q separately; only the effective contrast $c = Af_q^2$ will be considered. When Eq. (2) is used to describe the spontaneous dynamics in glasses and undercooled liquids, usually one finds $\beta \leq 1$, a sign of a heterogeneous dynamics [22]; however, it is not uncommon to observe $\beta > 1$ in arrested systems, which is considered as a signature of a stress-release mechanism [23–25]. In addition, the q dependence of the parameters of the KWW function gives precious information on the dynamics that the particles undergo. For example, in the case of Brownian diffusion, the relaxation time for the self-component of $F(q,t)$ scales as $\tau \propto 1/q^2$ [20], corresponding to a mean-squared displacement $\langle \Delta R(t)^2 \rangle \propto t$. For undercooled liquids, the parameters (τ, β) become almost q independent if not for a modulation in phase with the scattered intensity $I(q)$ [26]. For what concerns $\tau(q)$, this feature is usually referred to as the de Gennes narrowing effect [27], and it is a characteristic signature of collective dynamics. Finally, a ballistic behavior ($\tau \propto 1/q$) is usually rationalized in terms of a stress-induced velocity field that drives the dynamics [28,29].

Recent experiments carried out on oxide glasses have shown that XPCS is very sensitive to the defects generated by the x-ray beam in a pump-and-probe fashion [30–32]: Hard x-ray photons induce (pump), by photoelectric absorption, structural defects that result in structural rearrangements detected by photons of the same beam (probe). The typical time of this structural relaxation process scales inversely with the dose rate delivered to the sample, which is the hallmark of its induced nature [30]. However, a comprehensive understanding of the microscopic mechanisms behind this induced dynamics is still missing, as is the reason for clear qualitative differences between different materials [30,32–35].

Here, we exploit recent improvements of XPCS to shed some new light on this effect. We show that we are, in fact, witnessing a transition of general interest. In Fig. 1(a), we report a two-time correlation matrix for a $LiBO_2$ glass. We are in the presence of a nonstationary process. In fact, averaging the correlation matrix over different time intervals (colored squares), we obtain different $g_2(q,t)$ functions; see Fig. 1(b): At short t_w, the $g_2(q,t)$ function is compressed ($\beta > 1$), while at longer t_w, it becomes stably stretched ($\beta < 1$). The time-averaged function will clearly depend on the total integration time. Given the relatively low dose (short t_w) corresponding to the initial transient dynamics and the low-scattering cross section of borate glasses, it is not surprising that, in previous works [34,36], this effect was unnoticed. However, Fig. 1 demonstrates that a careful time- (or dose-) dependent study is required, as we discuss in the following.

A. Low-dose limit

Measuring density correlation functions in the low-dose limit, i.e., at doses corresponding to one characteristic decay time τ or less, is challenging. Usually, in fact, even

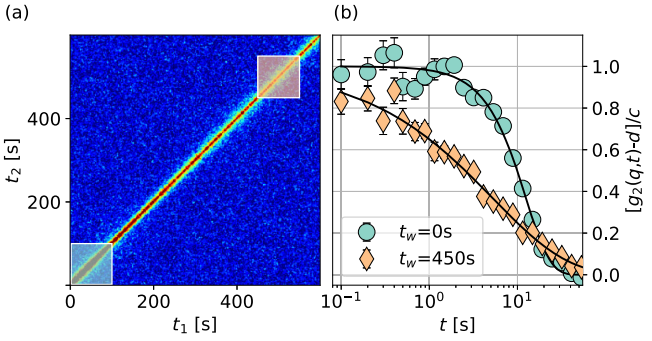

FIG. 1. (a) Two-time correlation matrix for a $LiBO_2$ glass at $q = (17.0 \pm 1.7)$ nm^{-1}. The two squares show two submatrices utilized to compute correlation functions at two different waiting times t_w. (b) Two correlation functions computed at short and long t_w, as shown in panel (a), reported after baseline, d, subtraction, and normalization to the initial contrast, c. KWW fits to the experimental data are also shown. These two functions have similar relaxation times τ [(19.5 ± 0.4) s and (20.3 ± 1.6) s, respectively] but different shape parameters β (1.57 ± 0.07 and 0.51 ± 0.05, respectively).

for a multispeckle detection scheme like the one adopted here [37], in order to reach an acceptable statistical quality, one needs to acquire a sequence of images over at least several tens of τ, which is something we need to avoid here. We then adopt a different scheme. We acquire a series of images during a time interval of one τ on a grid of points on the sample to gain by ensemble averaging what we cannot gain by time averaging.

Figure 2(a) presents a set of $g_2(q,t)$ for a selection of q values measured in this way. In order to correctly describe

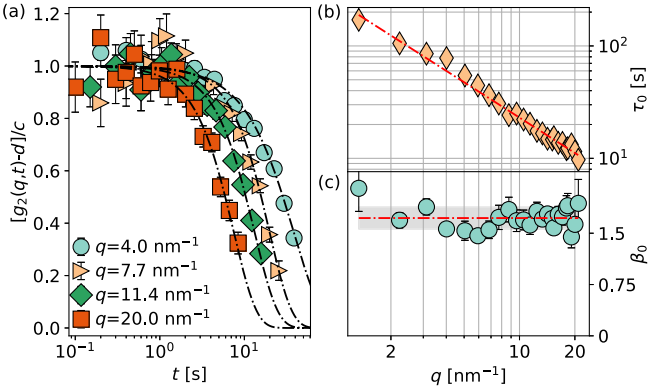

FIG. 2. (a) The $g_2(q,t)$ functions for a $LiBO_2$ glass in the low-dose limit for a selection of different exchanged wave vectors and for a total integration time of τ. The correlation functions are reported with the baseline, d, subtracted and after normalization to the experimental contrast, c. The black dashed-dotted lines are evaluated using the parameters reported in panels (b) and (c). (b) Low-dose relaxation time as a function of q. The power-law fit (red dashed line) corresponds to $\tau_0 \propto q^{-\alpha}$, with $\alpha = 1.05 \pm 0.02$. (c) Low-dose shape parameter β_0 as a function of q. The values of β_0 are q independent in the considered q range and have an average value of $\langle \beta_0 \rangle = 1.72 \pm 0.16$.

these correlation functions using the KWW ansatz, it is important to take into account the strong dose (or t_w) dependence of its parameters. Then, it is possible to access the low-dose limiting values for τ and β, τ_0 and β_0, respectively; see Supplemental Material [38] for more details. In Fig. 2(b), the obtained τ_0 values are reported as a function of q. Fitting a power law to the data, $\tau_0(q) = (bq^\alpha)^{-1}$, gives $\alpha = 1.05 \pm 0.02$ (red dashed line). Here, b is a coefficient proportional to the dose rate. Our data are then compatible with a decay time inversely proportional to q. The corresponding values for the shape parameter $\beta_0(q)$ are reported in Fig. 2(c). They are all compressed, $\beta_0 > 1$, and show no dependence on q. Their mean value is $\langle\beta_0\rangle = 1.72 \pm 0.16$, compatible with $3/2$ within 2 standard deviations. These results are interesting because the values $\alpha = 1$ and $\beta = 3/2$ are considered signatures of ballistic dynamics, as observed in many soft-matter systems [23,28,29,39–45] and in numerical simulations [46,47].

Given the similarity of our results with those reported in soft matter, we can exploit the approach developed in Ref. [28] to interpret the results of Fig. 2. In more detail, we can rewrite the density correlation function as

$$F(q,t) = e^{-[t/\tau_0(q)]^{\beta_0(q)}} = e^{-[btq]^{3/2}} = \langle e^{i\mathbf{q}\cdot\Delta\mathbf{R}(t)}\rangle. \quad (3)$$

Here, $\Delta\mathbf{R}(t)$ is the atomic displacement at time t, and the last equality is the expression of the intermediate-scattering function when it is approximated with its self-component [20]. Equation (3) allows us to use a simple model to describe the experimental data [23,28]. This model is based on a distribution of rare elastic dipoles (stress sources), which induce an atomic displacement field that scales as $\Delta\mathbf{R} \sim r^{-2}$, r being the distance from the dipole. In light-scattering experiments in soft matter, these stress sources arise spontaneously in the aging material [23]; here, the stress sources are the defects generated by x-ray absorption.

We have direct evidence for the generation of defects in our glasses upon x-ray exposure. At the end of the experiment, the samples, which were initially transparent, displayed clear color centers at the spots hit by the x-ray beam. This effect, quite common when irradiating transparent insulators, is a clear indication of the x-ray-induced generation of defects in these glasses. More generally, the generation of defects in lithium-borate glasses exposed to ionizing radiation is a well-known effect that has been investigated in detail [48,49]. In fact, given that the effective atomic number of lithium-borate glasses is quite similar to the tissue's value, the dependence of the number of generated defects on the radiation dose has driven research in the fields of clinical and personal dosimetry since the early 1970s [50]. Our samples are not exceptions in this regard, and evidence of the generation of optically active defects upon x-ray exposure is reported in the Supplemental Material [38].

Concluding this section, at low doses, we observe the effect of a diluted distribution of noninteracting defects, each behaving as a shear transformation zone described as an Eshelby inclusion, inducing an elastic displacement field. Our irradiated glass is only slightly modified by x-ray irradiation and still behaves like an elastic solid. At the microscopic scale, it corresponds to a glass under load in the low-stress limit of its stress-strain curve.

B. Increasing the dose

Figure 3 shows the exchanged momentum dependence of the relaxation time τ, panel (a), and shape parameter β, panel (b), for a few selected doses; see Supplemental Material [38] for some examples of the correlation functions used to extract these fit parameters. Upon increasing the irradiation time, β tends to decrease, accompanied by a weaker dependence of the relaxation time on q. After irradiation with a dose of close to 1 GGy, both $\tau(q)$ and $\beta(q)$ start to show a peak around the position of the maximum of $I(q)$ at $q \simeq 17$ nm^{-1}.

In order to clarify the origin of the dose dependence of the parameters reported in Fig. 3, we report in Fig. 4(a) the scattered intensity $I(q)$ over the investigated q range for a few selected doses. Small but clear changes can be observed on increasing the dose: The peak intensity decreases, and the main peak broadens, accompanied by an increase of intensity at small angles. These effects, qualitatively similar to those reported for a SiO_2 glass [30], suggest that the glass becomes more disordered as the irradiation proceeds: A larger distribution of interatomic distances (more disorder) can explain the slight broadening of the first peak in $I(q)$ while the increase of intensity at small angles suggests that the glass is rejuvenating under

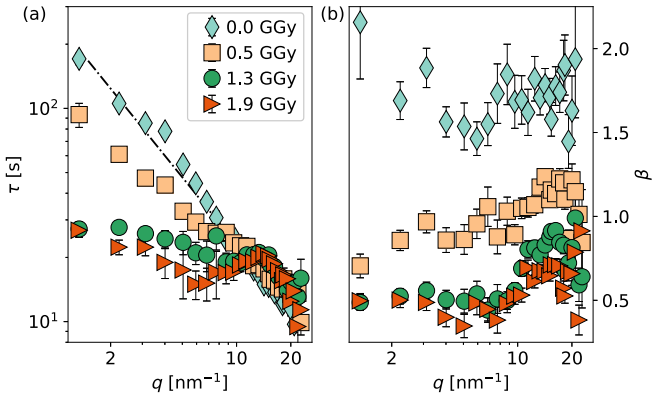

FIG. 3. (a) Relaxation time as a function of q for a few selected doses for a $LiBO_2$ glass. (b) Shape parameter as a function of q for the same doses as in panel (a). At high doses, a clear de Gennes narrowing effect can be observed in the q dependence of τ, and a related oscillation appears also in that of β. Light-blue diamonds are the low-dose limiting values τ_0 and β_0, and they correspond to a zero absorbed dose (see Supplemental Material [38]).

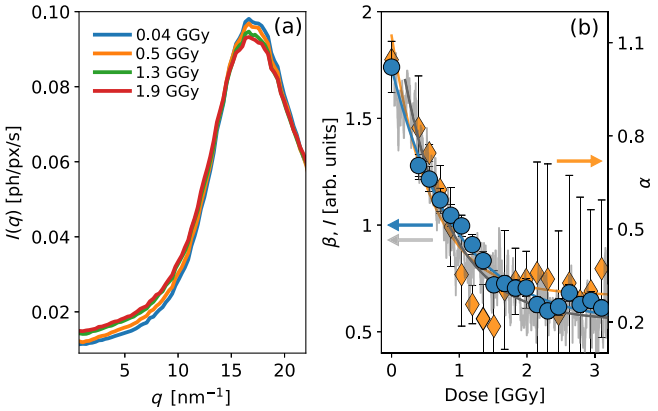

FIG. 4. (a) Scattered intensity for a few selected doses. (b) Left axis: shape parameter β (blue circles) together with the scattered intensity (gray line) as a function of the absorbed dose. Both data sets correspond to the exchanged wave vector $q = 17$ nm^{-1}. Right axis: fitted power-law exponent α (orange diamonds) as a function of the absorbed dose. Note that α has been extracted by fitting a power law to the q dependence of the relaxation time, $\tau = (bq^{\alpha})^{-1}$, in the range $2 \leq q \leq 6$ nm^{-1}, thus avoiding the de Gennes narrowing range.

the beam [51]. This result is clearly consistent with an increasing density of defects on increasing the dose and also with the computational observation that the defected regions are, in fact, rejuvenated with respect to the glass matrix [52].

It is interesting to compare the dose dependence of the scattered intensity with that of the relaxation time and shape parameter that describe the density correlation functions, as reported in Fig. 4(b). In particular, we report the dose dependence of β (blue circles), together with that of the intensity scattered at the peak of $I(q)$ (gray line) and of the coefficient α (orange diamonds) of the power law that describes the q dependence of τ at low q. Interestingly, all three quantities change on a very similar dose scale of around 1GGy. At doses somewhat higher than around 1.9 GGy, both the structure and the dynamics of the irradiated glass reach a stationary state, which we refer to in the following as the fully irradiated glass. Figure 4 thus shows that the changes in the density correlation function proceed together with the structural changes: Both are related to the continuous increase of the density of defects upon irradiation. We also observe that there seems to exist a maximum number of defects that can be generated in a glass by x-ray irradiation, and the glass with the maximum number of defects corresponds to the fully irradiated glass: For every newly generated defect, another one heals, like in a liquid at equilibrium.

Generalizing the approach that leads to Eq. (3), we can rewrite the intermediate-scattering function as

$$F(q,t) = e^{-(b^{\gamma}t^{\gamma}q)^{p}}, \tag{4}$$

where b is again a coefficient proportional to the dose rate, and where $\gamma = 1/\alpha$ and $p = \alpha\beta$ are extracted from the data reported in Fig. 3. This description is possible in the dose range where the parameters α and β are q independent, which corresponds, in the present case, to doses up to around 1 GGy.

In the low-dose limit, it was possible to use a simple model of noninteracting elastic dipoles to describe the functional form found for $F(q,t)$. At larger doses, where we expect a denser distribution of defects, that model does not hold any longer, but we can still obtain information on the displacement field. In fact, approximating the intermediate-scattering function with its self-component, it is possible to write [20]

$$F(q,t) = \langle e^{i\mathbf{q}\cdot\Delta\mathbf{R}(t)}\rangle = \int g(\Delta\mathbf{R}(t))e^{i\mathbf{q}\cdot\Delta\mathbf{R}(t)}\mathrm{d}(\Delta\mathbf{R}). \tag{5}$$

Here, $g(\Delta\mathbf{R}(t))$ is the distribution function of $\Delta\mathbf{R}(t)$ at time t, also known as the self-component of the van Hove function [20]. Starting from the knowledge of $F(q,t)$ that we measure, we can invert Eq. (5) to extract the function $w(\Delta R(t)) = 4\pi^2(\Delta R(t))^2 g(\Delta\mathbf{R}(t))$, which represents the distribution function of the modulus of $\Delta\mathbf{R}(t)$ [28]. The result is

$$w(\Delta R(t)) = -\frac{2\Delta R(t)}{(bt)^{\gamma}}\frac{\mathrm{d}}{\mathrm{d}(\Delta R)}L_{p,0}(\Delta R/(bt)^{\gamma}), \tag{6}$$

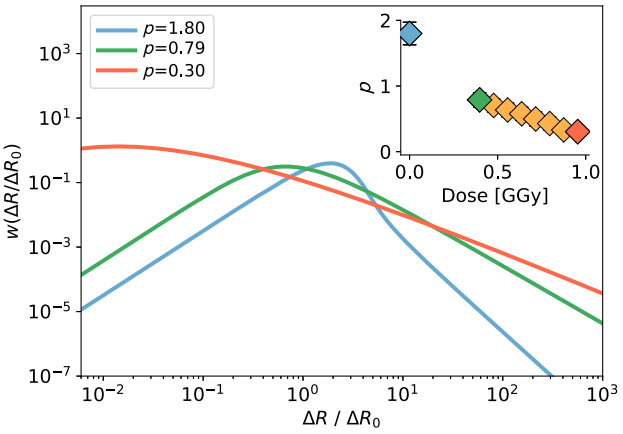

FIG. 5. Distribution function $w(\Delta R)$ of the modulus of the atomic displacements ΔR for different values of p (different doses). The tail of the distribution becomes more and more pronounced on decreasing the p value: Long displacements become more and more probable on increasing the absorbed dose. The distributions are reported as a function of normalized displacements, where $\Delta R_0 = (bt)^{\gamma}$. Inset: dose dependence of the coefficient p. Three points (blue, green, and red diamonds) correspond to the functions reported in the main figure. For each dose, the p value is calculated using the corresponding value of the shape parameter β, together with the q dependence of the relaxation time.

where $L_{p,0}$ is the Lévy stable law, characterized by an asymptotic power-law decay: $L_{p,0} \sim (\Delta R)^{-(p+1)}$ [20,28]. This approach allows us to interpret the dose dependence of the parameters τ and β in terms of changes in the distribution of atomic displacements, which is shown in Fig. 5, where we report the function $w(\Delta R)$ evaluated for a selection of coefficients $p = \alpha\beta$ among those reported in the inset. The coefficient p decreases monotonically from the low-dose value compatible with that typical of an elastic displacement field generated by a distribution of isolated defects, i.e., $p = 3/2$, to a smaller value close to 0. Small values of p are delicate as they imply a distribution of displacements with undefined mean and variance. This is likely a consequence of the limited q range over which the XPCS experiment has been carried out and thus of the limited q range used to Fourier transform the measured intermediate-scattering function to obtain the distribution of the atomic displacements. In other terms, the power-law dependencies corresponding to small values of p reported in Fig. 5 cannot last forever; rather, they must feature a cutoff somewhere that could possibly be reached by increasing the q range over which the XPCS experiment is carried out. Still, the tendency of the tail of the distribution of displacements to flatten, at least in the vicinity of its peak, upon increasing the dose is an interesting observation. A smaller value of p corresponds to a fatter tail of the Lévy stable distribution that enters Eq. (6) and thus to a larger probability for displacements to larger distances. This trend is consistent with the idea that, on increasing the density of plastic regions and thus in a more disrupted network, larger displacements are more and more facilitated, though they remain clearly nondiffusive.

For doses larger than about 1 GGy, the de Gennes narrowing effect starts to appear in the q dependence of τ, a sign that collective effects start to play a more and more relevant role in the dynamics. The approximation leading to Eq. (6) in the glass irradiated with a low dose cannot hold any longer: In the glass irradiated with a high dose, we no longer probe the displacement of a single particle; instead, a correlated atomic motion dominates the density fluctuations.

C. Glass at the yield point

The dynamical properties of the fully irradiated glass show strong similarities with experimental and simulation results for undercooled liquids: an almost q-independent decay time τ displaying the de Gennes narrowing effect [27] and a stretching parameter $\beta < 1$ oscillating in phase with the structure factor [26]. Actually, the comparison between the shape of the density correlation function for the fully irradiated glass and for the liquid can be taken much further.

In Fig. 6(a), we compare the $g_2(q,t)$ function for the fully irradiated glass (corresponding to a dose of 1.9 GGy) and for the undercooled liquid measured with both XPCS and dynamic light scattering; see Supplemental Material [38] for more details. The shape parameter for the fully irradiated glass matches the one of the undercooled liquid ($\beta = 0.57 \pm 0.04$), as confirmed by the fact that all curves overlap. Moreover, in Fig. 6(b), the q dependence of the (normalized) relaxation time for the fully irradiated $LiBO_2$ glass is shown, together with the one of the undercooled liquid. They are also very close to each other, and both display the de Gennes narrowing effect. In other terms, the density correlation function at the interatomic length scale of a fully irradiated glass is very similar to that of a liquid, both in terms of q dependence of τ and in terms of β. We expect that this striking similarity will break down at sufficiently low q, i.e., at the macroscopic scale, where the difference between a liquid and the irradiated glass should be clear.

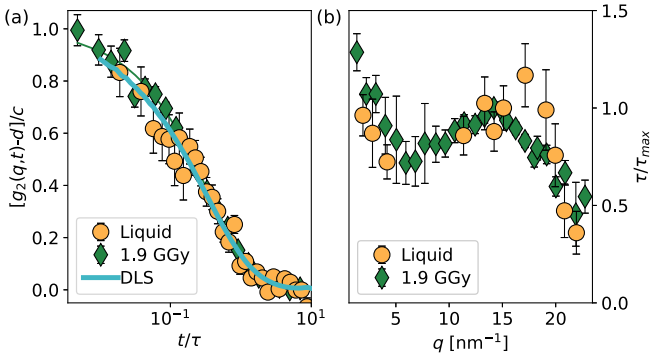

FIG. 6. (a) The $g_2(q,t)$ functions plotted in terms of time scaled by the decay time for a fully irradiated glass (absorbed dose of 1.9 GGy, green diamonds) and for the undercooled liquid at $T =$ 708 K (orange circles). The continuous cyan line is for dynamic light-scattering data at 738 K. The $g_2(q,t)$ functions are reported after subtraction of the baseline and normalization to the experimental contrast. (b) Relaxation time as a function of the exchanged wave vector q for the same fully irradiated glass and supercooled liquid as in panel (a), same symbols. Both data sets have been normalized in order to emphasize the similarity of their q dependence. The values used for the normalization are $\tau_{max} =$ 20.9 s at $q = 14.2$ nm^{-1} for the fully irradiated glass and 4.3 s at $q = 15.1$ nm^{-1} for the undercooled liquid.

In the fully irradiated glass, we are witnessing the structural relaxation that follows the generation of a defect. However, the density of defects is so high that the way the system reacts to this novel defect is very close to how a spontaneous fluctuation relaxes in a liquid: The matrix is no longer elastic but flows; we are at the yield point. Here, this very special point, which is crossed abruptly in a standard stress-strain experiment, becomes a stationary state during x-ray irradiation at a sufficiently high dose.

Clearly, the yield point reached by irradiation is not the same yield point reached in stress-strain experiments. In fact, it cannot be: The fully irradiated glass reached here does not flow macroscopically while a glass loaded beyond the yield stress does. Still, these two approaches both lead to yielding; i.e., in both cases, the obtained glasses display a fully plastic response following a density fluctuation.

III. CONCLUSIONS

Here, we have shown that the entire transition of a glass from the elastic limit to the yielding point that is traditionally realized in stress-strain experiments can alternatively be realized at (almost) constant volume by increasing the density of plastic regions (defects) upon x-ray irradiation. The amorphous states at yield and along the whole transition between the elastic limit and the yield point reached by these two approaches are different, thus offering a new approach to a difficult problem under current scrutiny, that of the mechanical properties of amorphous materials in the plastic regime at the microscopic scale [2]. We expect that the detailed comparison between the sequence of amorphous structures reached with these two approaches will be particularly rich in information. In particular, the control of the density of plastic regions generated by irradiation and the simultaneous microscopic characterization by XPCS of the elasto-plastic response of glasses can provide information currently impossible to achieve experimentally with other, more traditional schemes. In the way it has been used here, XPCS amounts to a tool to probe the mean atomic dynamics in a glass with an increasing density of defects. As such, it complements the continuous developments to obtain similar information by imaging techniques [53] but with the unique advantage of providing statistically robust results at the interatomic scale.

One clear specific point of interest in our experimental approach is the possibility to design the distribution of defects in a glass by the appropriate choice of the x-ray beam profile and/or by an appropriate distribution of x-ray-absorbing atoms in the glass. This should be compared with the stochastic appearance of plastic regions in a strained glass. This advantage can be exploited to study the interaction of defects in a controlled way, which can be relevant for the development of more refined theories or models. More generally, the dose can be controlled very accurately, and therefore, the approach to the yield point and beyond can be followed in small steps, contrasted with the very abrupt mechanical failure that is reached in standard stress-strain experiments for brittle materials like glasses. While in the present experiment XPCS has been used to explore a q range that covers slightly more than a decade, a much larger q range, maybe covering up to three decades or more, can be explored in an optimized experiment. This approach can then be very useful to provide feedback to the development of novel theories describing the mechanical properties of amorphous materials with a high density of plastic regions as, e.g., the recent theory of screened elasto-plasticity [16,54].

ACKNOWLEDGMENTS

Parts of this research were carried out at beamline P10 (experiment I-20190834EC) at DESY, a member of the Helmholtz Association (HGF). The research leading to the results has been supported by the project CALIPSOplus under the European Union's Horizon 2020 research and innovation program (Grant Agreement No. 730872) and by the project GLAXES ERC-2021-ADG (Grant Agreement No. 101053167) funded by the European Union. F. C. is a charge de recherches of the Fonds de la Recherche Scientifique FNRS.

Author contributions: A. M. and G. M. designed the research; A. M., F. C., F. D., M. S., F. W., G. B., and G. M. performed the experiments; A. M. analyzed the data; A. M. and G. M. wrote the paper, with contributions from all authors.

The authors declare no competing interest.

APPENDIX

1. $LiBO_2$ glasses

The glasses used here were prepared by melt quenching, with lithium carbonate (Li_2CO_3, 99.9% purity) and anhydrous boron oxide (B_2O_3, 99% purity) as starting materials, both purchased from Sigma-Aldrich. More specifically, a few grams of these materials were placed in a furnace (temperature stability ± 1 K) and heated to 398 K for 24 hours. This baking is essential to remove water and then correctly weight the amount of Li_2CO_3 and B_2O_3 needed to reach the target alkali molar fraction. The dried powders were mixed and melted in an alumina crucible at 1273 K for 4.5 hours. The melt was then quenched by pressing it between stainless-steel plates preheated at 473 K. The obtained glass was annealed below the tabulated glass transition temperature [55] for 6 hours and then cooled down to room temperature at a rate of 0.5 K/min. Eventually, the samples were cut in the shape of disks and polished to the desired thickness with abrasive paper.

2. XPCS experiment

The XPCS experiment was performed at beamline P10 of the PETRA III storage ring in Hamburg (Germany). A beam of 8.4 keV photons ($\lambda = 1.476$Å) was monochromatized with a Si(111) channel-cut crystal and focused with beryllium compound refractive lenses onto a spot of 1.9×2.7 μm^2 (V × H) full width half maximum (FWHM). The sample was mounted in vacuum, and the scattered intensity was collected at different scattering angles ($\theta \sim 2° - 30°$) using an EIGER 4M detector mounted on a goniometer arm.

The photon flux was measured with a calibrated photodiode placed downstream of the sample, and the obtained result was $F_0 = 5.7 \times 10^{10}$ ph/s, with 100 mA of current in the storage ring. The absorbed dose was calculated considering an elliptical beam cross section, with semiaxes equal to the corresponding FWHM/$\sqrt{2\ln(2)}$ values. The

dose rate used for this experiment is then 4 MGy for 1 s of exposure. The samples of lithium metaborate glasses, $LiBO_2$, were prepared with thicknesses W ∼ 100–150 μm. These values, despite being well below the attenuation length at the x-ray beam wavelength ($\mu = 683$ μm), are a reasonable compromise to reach a high enough speckle contrast and a high enough intensity in the wide-angle scattering range. The XPCS measurements were performed at room temperature as a function of the dose. One set of measurements was collected above the glass transition temperature in the undercooled liquid state (T = 708 K). For that measurement, a furnace under vacuum was used to reach the temperature of interest.

[1] C. A. Schuh, T. C. Hufnagel, and U. Ramamurty, *Mechanical behavior of amorphous alloys*, Acta Mater. **55**, 4067 (2007).

[2] A. Nicolas, E. E. Ferrero, K. Martens, and J.-L. Barrat, *Deformation and flow of amorphous solids: insights from elastoplastic models*, Rev. Mod. Phys. **90**, 045006 (2018).

[3] P. K. Jaiswal, I. Procaccia, C. Rainone, and M. Singh, *Mechanical yield in amorphous solids: A first-order phase transition*, Phys. Rev. Lett. **116**, 085501 (2016).

[4] P. Leishangthem, A. D. S. Parmar, and S. Sastry, *The yielding transition in amorphous solids under oscillatory shear deformation*, Nat. Commun. **8**, 14653 (2017).

[5] M. Ozawa, L. Berthier, G. Biroli, A. Rosso, and G. Tarjus, *Random critical point separates brittle and ductile yielding transitions in amorphous materials*, Proc. Natl. Acad. Sci. U.S.A. **115**, 6656 (2018).

[6] S. Karmakar, E. Lerner, and I. Procaccia, *Athermal nonlinear elastic constants of amorphous solids*, Phys. Rev. E **82**, 026105 (2010).

[7] A. Argon, *Plastic deformation in metallic glasses*, Acta Metall. **27**, 47 (1979).

[8] J. Ding, S. Patinet, M. L. Falk, Y. Cheng, and E. Ma, *Soft spots and their structural signature in a metallic glass*, Proc. Natl. Acad. Sci. U.S.A. **111**, 14052 (2014).

[9] M. L. Falk and J. S. Langer, *Dynamics of viscoplastic deformation in amorphous solids*, Phys. Rev. E **57**, 7192 (1998).

[10] J. D. Eshelby, *The determination of the elastic field of an ellipsoidal inclusion, and related problems*, Proc. R. Soc. A **241**, 376 (1957).

[11] R. Dasgupta, H. G. E. Hentschel, and I. Procaccia, *Microscopic mechanism of shear bands in amorphous solids*, Phys. Rev. Lett. **109**, 255502 (2012).

[12] P. Schall, D. A. Weitz, and F. Spaepen, *Structural rearrangements that govern flow in colloidal glasses*, Science **318**, 1895 (2007).

[13] E. D. Knowlton, D. J. Pine, and L. Cipelletti, *A microscopic view of the yielding transition in concentrated emulsions*, Soft Matter **10**, 6931 (2014).

[14] A. Ghosh, Z. Budrikis, V. Chikkadi, A. L. Sellerio, S. Zapperi, and P. Schall, *Direct observation of percolation in the yielding transition of colloidal glasses*, Phys. Rev. Lett. **118**, 148001 (2017).

[15] A. Lemaître, C. Mondal, M. Moshe, I. Procaccia, S. Roy, and K. Screiber-Re'em, *Anomalous elasticity and plastic screening in amorphous solids*, Phys. Rev. E **104**, 024904 (2021).

[16] B. P. Bhowmik, M. Moshe, and I. Procaccia, *Direct measurement of dipoles in anomalous elasticity of amorphous solids*, Phys. Rev. E **105**, L043001 (2022).

[17] E. Garman and M. Weik, *Radiation damage to biological samples: Still a pertinent issue*, J. Synchrotron Radiat. **28**, 1278 (2021).

[18] T. Narayanan, M. Sztucki, T. Zinn, J. Kieffer, A. Homs-Puron, J. Gorini, P. Van Vaerenbergh, and P. Boesecke, *Performance of the time-resolved ultra-small-angle x-ray scattering beamline with the extremely brilliant source*, J. Appl. Crystallogr. **55**, 98 (2022).

[19] G. Grübel and F. Zontone, *Correlation spectroscopy with coherent x-rays*, J. Alloys Compd. **362**, 3 (2004).

[20] B. J. Berne and R. Pecora, *Dynamic Light Scattering: With Applications to Chemistry, Biology, and Physics* (Dover Publications, New York, 1976).

[21] G. Williams and D. C. Watts, *Non-symmetrical dielectric relaxation behaviour arising from a simple empirical decay function*, Trans. Faraday Soc. **66**, 80 (1970).

[22] E. Vidal Russell and N. Israeloff, *Direct observation of molecular cooperativity near the glass transition*, Nature (London) **408**, 695 (2000).

[23] L. Cipelletti, S. Manley, R. Ball, and D. Weitz, *Universal aging features in the restructuring of fractal colloidal gels*, Phys. Rev. Lett. **84**, 2275 (2000).

[24] B. Ruta, Y. Chushkin, G. Monaco, L. Cipelletti, E. Pineda, P. Bruna, V. Giordano, and M. Gonzalez-Silveira, *Atomic-scale relaxation dynamics and aging in a metallic glass probed by x-ray photon correlation spectroscopy*, Phys. Rev. Lett. **109**, 165701 (2012).

[25] B. Ruta, G. Baldi, G. Monaco, and Y. Chushkin, *Compressed correlation functions and fast aging dynamics in metallic glasses*, J. Chem. Phys. **138**, 054508 (2013).

[26] B. Ruta, S. Hechler, N. Neuber, D. Orsi, L. Cristofolini, O. Gross, B. Bochtler, M. Frey, A. Kuball, S. S. Riegler, M. Stolpe, Z. Evenson, C. Gutt, F. Westermeier, R. Busch, and I. Gallino, *Wave-vector dependence of the dynamics in supercooled metallic liquids*, Phys. Rev. Lett. **125**, 055701 (2020).

[27] P. G. De Gennes, *Liquid dynamics and inelastic scattering of neutrons*, Physica **25**, 825 (1959).

[28] L. Cipelletti, L. Ramos, S. Manley, E. Pitard, D. A. Weitz, E. E. Pashkovski, and M. Johansson, *Universal non-diffusive slow dynamics in aging soft matter*, Faraday Discuss. **123**, 237 (2003).

[29] F. Dallari, A. Martinelli, F. Caporaletti, M. Sprung, G. Grübel, and G. Monaco, *Microscopic pathways for stress relaxation in repulsive colloidal glasses*, Sci. Adv. **6**, eaaz2982 (2020).

[30] B. Ruta, F. Zontone, Y. Chushkin, G. Baldi, G. Pintori, G. Monaco, B. Ruffle, and W. Kob, *Hard x-rays as pump and probe of atomic motion in oxide glasses*, Sci. Rep. **7**, 3962 (2017).

[31] F. Dallari, A. Martinelli, F. Caporaletti, M. Sprüng, G. Baldi, and G. Monaco, *Stochastic atomic acceleration during the x-ray induced fluidization of a silica glass*, Proc. Natl. Acad. Sci. U.S.A. **120**, e2213182120 (2023).

[32] E. Alfinelli, F. Caporaletti, F. Dallari, A. Martinelli, G. Monaco, B. Ruta, M. Sprung, M. Zanatta, and G. Baldi, *Amorphous-amorphous transformation induced in glasses by intense x-ray beams*, Phys. Rev. B **107**, 054202 (2023).

[33] G. Pintori, G. Baldi, B. Ruta, and G. Monaco, *Relaxation dynamics induced in glasses by absorption of hard x-ray photons*, Phys. Rev. B **99**, 224206 (2019).

[34] K. Holzweber, C. Tietz, T. M. Fritz, B. Sepiol, and M. Leitner, *Beam-induced atomic motion in alkali borate glasses*, Phys. Rev. B **100**, 214305 (2019).

[35] F. Dallari, G. Pintori, G. Baldi, A. Martinelli, B. Ruta, M. Sprung, and G. Monaco, *X-rays induced atomic dynamics in a lithium-borate glass*, Condens. Matter Phys. **22**, 43606 (2019).

[36] G. Pintori, G. Baldi, F. Dallari, A. Martinelli, M. Sprung, and G. Monaco, *X-ray induced dynamics in borate glasses with different network connectivity*, Phys. Rev. B **105**, 104207 (2022).

[37] L. Cipelletti and D. A. Weitz, *Ultralow-angle dynamic light scattering with a charge coupled device camera based multispeckle, multitau correlator*, Rev. Sci. Instrum. **70**, 3214 (1999).

[38] See Supplemental Material at http://link.aps.org/supplemental/10.1103/PhysRevX.13.041031 for more information.

[39] P. Falus, M. Borthwick, S. Narayanan, A. Sandy, and S. Mochrie, *Crossover from stretched to compressed exponential relaxations in a polymer-based sponge phase*, Phys. Rev. Lett. **97**, 066102 (2006).

[40] A. Madsen, R. L. Leheny, H. Guo, M. Sprung, and O. Czakkel, *Beyond simple exponential correlation functions and equilibrium dynamics in x-ray photon correlation spectroscopy*, New J. Phys. **12**, 055001 (2010).

[41] R. Angelini, L. Zulian, A. Fluerasu, A. Madsen, G. Ruocco, and B. Ruzicka, *Dichotomic aging behaviour in a colloidal glass*, Soft Matter **9**, 10955 (2013).

[42] R. Angelini and B. Ruzicka, *Non-diffusive dynamics in a colloidal glass: Aging versus rejuvenation*, Colloids Surf. **483**, 316 (2015).

[43] A. Duri and L. Cipelletti, *Length scale dependence of dynamical heterogeneity in a colloidal fractal gel*, Europhys. Lett. **76**, 972 (2006).

[44] V. Trappe, E. Pitard, L. Ramos, A. Robert, H. Bissig, and L. Cipelletti, *Investigation of q-dependent dynamical heterogeneity in a colloidal gel by x-ray photon correlation spectroscopy*, Phys. Rev. E **76**, 051404 (2007).

[45] A. Jain, F. Schulz, I. Lokteva, L. Frenzel, G. Grübel, and F. Lehmkühler, *Anisotropic and heterogeneous dynamics in an aging colloidal gel*, Soft Matter **16**, 2864 (2020).

[46] M. Bouzid, J. Colombo, L. V. Barbosa, and E. Del Gado, *Elastically driven intermittent microscopic dynamics in soft solids*, Nat. Commun. **8**, 15846 (2017).

[47] N. Gnan and E. Zaccarelli, *The microscopic role of deformation in the dynamics of soft colloids*, Nat. Phys. **15**, 683 (2019).

[48] D. Griscom, *ESR studies of radiation damage and structure in oxide glasses not containing transition group ions: A contemporary overview with illustrations from the alkali borate system*, J. Non-Cryst. Solids **13**, 251 (1974).

[49] I. A. Shkrob, B. M. Tadjikov, and A. D. Trifunac, *Magnetic resonance studies on radiation-induced point defects in mixed oxide glasses. I. Spin centers in* B_2O_3 *and alkali borate glasses*, J. Non-Cryst. Solids **262**, 6 (2000).

[50] P. Almond, K. McCray, and D. Espejo, *A lithium borate thermoluminescent dosimetry system for radiologic physics dosimetry*, Am. J. Roentgenol. **108**, 197 (1970).

[51] C. Levelut, A. Faivre, R. Le Parc, B. Champagnon, J.-L. Hazemann, and J.-P. Simon, *In situ measurements of density fluctuations and compressibility in silica glasses as a function of temperature and thermal history*, Phys. Rev. B **72**, 224201 (2005).

[52] A. D. S. Parmar, S. Kumar, and S. Sastry, *Strain localization above the yielding point in cyclically deformed glasses*, Phys. Rev. X **9**, 021018 (2019).

[53] A. Weidner and H. Biermann, *Review on strain localization phenomena studied by high-resolution digital image correlation*, Adv. Eng. Mater. **23**, 2001409 (2021).

[54] A. Lemaître, C. Mondal, M. Moshe, I. Procaccia, S. Roy, and K. Screiber-Re'em, *Anomalous elasticity and plastic screening in amorphous solids*, Phys. Rev. E **104**, 024904 (2021).

[55] J. Shelby, *Thermal expansion of alkali borate glasses*, J. Am. Ceram. Soc. **66**, 225 (1983).